The Structure, Stability, and Reactivity of Mo-oxo Species in H-ZSM5 Zeolites: Density Functional Theory Study

ARTICLE *in* THE JOURNAL OF PHYSICAL CHEMISTRY C · FEBRUARY 2007

Impact Factor: 4.77 · DOI: 10.1021/jp0640934

5 AUTHORS, INCLUDING:

Danhong Zhou
Liaoning Normal University
33 PUBLICATIONS **418** CITATIONS
SEE PROFILE

Ding Ma
Huazhong Univ Sci & Technol, Tongji Hosp, T…
308 PUBLICATIONS **3,224** CITATIONS
SEE PROFILE

The Structure, Stability, and Reactivity of Mo-oxo Species in H-ZSM5 Zeolites: Density Functional Theory Study

Danhong Zhou,*,†,‡ Yuan Zhang,† Hongyuan Zhu,† Ding Ma,‡ and Xinihe Bao*,‡

Institute of Chemistry for Functionalized Materials, College of Chemistry and Chemical Engineering, Liaoning Normal University, Dalian 116029, People's Republic of China, and State Key Laboratory of Catalysis, Dalian Institute of Chemical Physics, The Chinese Academy of Science, Dalian 116023, People's Republic of China

Received: June 29, 2006; In Final Form: November 14, 2006

The geometry and binding characteristic of Mo-oxo species anchored in the channels of H-ZSM5 zeolites were investigated by the density functional theory (DFT) method. The structures of the $(MoO_2)^{2+}$ monomer and the $(Mo_2O_5)^{2+}$ dimer were optimized based on the 6T cluster model. The calculations revealed that the $(Mo_2O_5)^{2+}$ dimer preferred to form at the next-next-near-neighbor-positioned Brönsted acid sites. The calculated Raman vibrational frequencies are in good agreement with the experimental result. The binding characteristics and electronic configurations of the $(MoO_2)^{2+}$ monomer and the $(Mo_2O_5)^{2+}$ dimer were examined by using natural bond orbital (NBO) analysis. The HOMO (highest occupied molecular orbital) in $(Mo_2O_5)^{2+}$/ZSM5 is related to the p orbital of the framework oxygen, whereas the LUMO (lowest unoccupied molecular orbital) is assigned to the antibonded π orbital of the Mo≡O triple bond. The reactivity of the $(Mo_2O_5)^{2+}$ dimer toward methane C−H bond dissociation was examined, and the transition state was determined with an activation energy of 63.5 kcal/mol.

1. Introduction

Direct conversion of methane to useful industrial products remains a formidable challenge. During the last 20 years, great attention has been focused on the molybdenum-loaded H-ZSM5 catalyst, which was confirmed to be the most effective catalyst for nonoxidative conversions of methane to aromatics with high benzene selectivity.[1−6] Several studies have clarified that the channel structure and the acidity of zeolites as well as the valence states and location of Mo species in H-ZSM5 are crucial factors for good catalytic performance of the catalyst.[7−12] Nevertheless, the distribution and the structural state of Mo species are always the hot point of research works.

Experimentally, two kinds of methods were generally used for the preparation of Mo/ZSM5 catalysts. One is the solid-state exchange from physical mixtures of MoO_3 and H-ZSM5 powders;[3] another is the impregnation or ion exchange of H-ZSM5 with aqueous ammonium heptamolybdate (AHM, $(NH_4)_6Mo_7O_{24}$) solution. By calcinations of the sample at 773−973 K, either small MoO_x species or $MoO_2(OH)_2$, which may result from the decomposition of AHM,[14,15,16] can migrate into zeolite channels and react with framework bridging hydroxyl groups to form $MoO_2(OH)^+$ species.[13] At even higher temperatures, $MoO_2(OH)^+$ species react with either vicinal Brönsted acidic protons or other $MoO_2(OH)^+$ groups to evolve H_2O and to form the anchored Mo monomers or dimers within zeolite channels. Using Monte Carlo simulations, we have confirmed that the tetrahedral-coordinated $MoO_2(OH)_2$ molecule should be the possible mobile Mo species in ZSM5 zeolite channels.[17]

Great efforts have been made to elucidate the nature of the Mo-oxo species, which are confirmed to be the precursor of molybdenum carbide, and to explore the possible mechanism of the reaction.[2,9,10,18−24] However, it is difficult to distinguish the Mo species of residual isolated MoO_x on the zeolite external surface and the Mo species anchored inside the zeolite channels; the location and the local structure of loaded Mo species remains controversial.

Bao and co-workers have studied the structure of Mo-oxo species using high-field solid-state NMR as well as the ab initio DFT method and proposed a monomer model.[25,26] In the proposed monomer model, a strong interaction between guest and zeolite occurs in a metal/zeolite system, with the molybdenum anchored to the framework Al through two oxygen bridges. Iglesia and co-workers[12,27−30] have characterized the structure of Mo-oxo species using Raman and X-ray absorption spectroscopy and suggested that the local structure of the MoO_x species in the exchanged sample was similar to the ditetrahedral structure of the isolated dimolybdate species in $MgMo_2O_7$.[12] The proposed structure of $(Mo_2O_5)^{2+}$ requires that the framework oxygens connected to Al atoms reside within 4.2−5.5 Å of each other. That is to say that the existence of either next-nearest-neighbor-positioned (NNN) Brönsted acid (B-acid) sites or next-next-nearest-neighbor-positioned (NNNN) B-acid sites should be crucial for the formation of the Mo dimer. Study from Bell's group on the occupation of T sites by Al as a function of the Si/Al ratio further supports the necessity of forming a dimer to overcome the long distance between two Al when the Si/Al ratio is >25.[31] Very recently, Louis and co-workers[32] reported that with a lower Si/Al ratio (about 15) two acidic protons were replaced by one Mo atom to form a monomeric $(MoO_2)^{2+}$ species bonded to two framework oxygens, similar to the structure observed in HY zeolite.[33] When the Si/Al ratio was higher, the distance between two B-acid sites became too long to build such a bidentate complex; therefore, a dimeric Mo complex was produced via condensation of two monomeric

* Corresponding authors. E-mail: dhzhou@dicp.ac.cn; xhbao@dicp.ac.cn.
† Liaoning Normal University.
‡ The Chinese Academy of Science.

10.1021/jp0640934 CCC: $37.00
Published on Web 01/11/2007

species to overcome the distance between the two grafting sites. Because the Mo-oxo species is the precursor of the MoC_x species,[27] which is confirmed to be the real catalysts for methane conversion to hydrocarbons,[9−10,12,30,34,35] it is necessary to investigate the structure and activity of the Mo-oxo species.

Although many experimental studies have offered some information on Mo-oxo/zeolite systems, questions such as why the Mo species associated with B-acid sites in zeolite display the catalytic activity have yet not been explained. Quantum chemical calculations can help us to acquire more understanding for the geometry and electronic structure of Mo-oxo species. Nevertheless, fewer reports about the theoretical studies on this system have been published so far.

In this paper, we focus on the geometric and electronic structures of the $(MoO_2)^{2+}$ monomer and the $(Mo_2O_5)^{2+}$ dimer associated with B-acid sites in H-ZSM5 by using the density functional theory (DFT) approach. Natural bond orbital (NBO) analyses were performed to examine the binding characteristics and molecular orbital configurations on optimized Mo-oxo models, and Raman vibrational frequencies were calculated and compared with experimental results. The activity of the $(Mo_2O_5)^{2+}$ dimer for methane C−H bond dissociation was studied. In contrast to other experimental studies on the MoO_x species, our theoretical calculations focus on the local structure of zeolite frameworks that account for the formation of stable Mo-oxo species, which can be considered strictly by truncating appropriate cluster models from the zeolite lattice. On the basis of the optimized structure of the Mo-oxo model, we can perform a detailed analysis of its electronic structure and energetics.

2. Methodologies

2.1. Calculation Methodology. All calculations were carried out with the DFT method by running the Gaussian 03 program[36] and DMol3 module in Material Studio software.[37] We began the geometry optimizations with different functionals by running DMol3. The LDA functionals of PWC[38] and NLDA functionals of PW91[38] and BLYP[39,40] were selected. The DNP (double numerical polarized) basis set was used for H, O, Si, and Al element, which corresponds to 6-31G** of the Gaussian orbital basis set, and is even more accurate than the same level basis set of Gaussian.[41,42] For the Mo atom, the effective core potential (ECP) was selected,[43,44] in which the inner shell electrons of Mo were substituted by the $[Ar]3d^{10}$ core, so we could treat the outer shell electrons (4s, 4p, 4d, 5s) only. After that, we carried out the geometry optimization using the hydride B3LYP functional (available in Gaussian 03), which led to more reasonable geometries and energies as compared with other LDA and NLDA methods. Therefore, the sequent calculations for electronic structure analyses and Raman vibrational frequencies were performed at the B3LYP/6-31G** level with the LanL2DZ ECP basis set for the Mo atom. For all optimized structures, the stationary points were verified by frequency calculations and no vibrational imaginary frequencies existed for optimized parts, except the contaminations of imaginary frequencies related to the constrained atoms. An averaging scaling factor[45] of 0.961 was used to correct the calculated frequencies for comparison with experiments. Natural bond orbital (NBO) calculations[46−48] were performed with the NBO code (version 3.2) included in Gaussian 03.[36]

2.2. Model Selection. In ZSM5 zeolite, there are 12 unique tetrahedral sites (referred to as T sites, T1−T12) per unit cell.[49] The Al atoms can replace some of the framework Si atoms; each Al site introduces one negative charge to the system, which is balanced by H^+, denoted as B-acid sites; and the Si/Al ratio

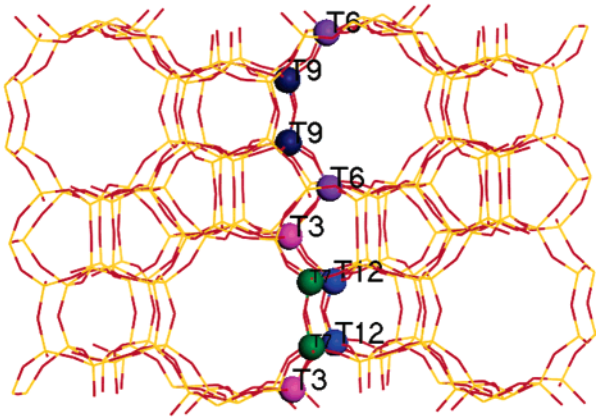

Figure 1. Structure of ZSM5 zeolite in the view of [100] with labeled adjacent T sites.

can be controlled by synthesis. The commonly synthesized H-ZSM5 zeolites bear a Si/Al ratio of 30−15, corresponding to Al atom numbers of 3−6 in a unit cell. The possible localizations of the exchanged Mo species were screened based on the following considerations: (1) Al atoms occupy the favorable T sites; and (2) the framework oxygen (O_F) atoms in adjacent B-acid sites must reside within 4.2−5.5 Å of each other.[12] As suggested by other authors, the favorable substituted Al located at T6, T9, and T12 sites in H-ZSM5 zeolite.[50] Therefore, our studies focused on these B-acid sites. We examined different possible O_F pairs in ZSM5 zeolite and found five locations, T3−T3, T3−T12, T6−T6, T6−T9, which locate at the intersections of channel systems, and T7−T12 locates in cross channels (Figure 1). These positions are attributed to NNN-acid sites (T6−T9 and T3−T12) and NNNN-acid sites (T6−T6, T3−T3, and T7−T12), respectively. The corresponding 6T cluster models (consisting of six T sites) were truncated from the ZSM5 zeolite lattice, which were denoted as T3T3, T3T12, T6T6, and T6T9, respectively, with T representing the corresponding Al substituted T sites. The dangling bond on the second shell framework oxygen atom was terminated by a H atom with an O−H distance fixed at 1.00 Å long and oriented along the bond direction to what would otherwise have been the next silicon atom. However, we had to choose the 10T cluster model for T7T12 because it is situated in a unique local environment. Using the 10T model, one can avoid problems such as two framework oxygen atoms linking with a mutual silicon atom, which results in introducing terminal OH groups that are too close. In the 10T model, the terminal Si−H bond was fixed at 1.460 Å long. During the calculations, all boundary terminal OH groups in 6T models were fixed in their original crystallographic positions, whereas overall 28 terminal atoms in the 10T model were fixed in order to retain the zeolite structures. Other atoms, including the MoO_x species, were calculated. The structure of the $Mo_2O_5(OH)_2$ molecule was constructed and optimized. Then, the Mo_2O_5 moiety was truncated and grafted onto zeolite cluster models to build Mo dimer models, which were then optimized by running DFT calculations.

3. Results and Discussions

3.1. Geometric Structure of the $(Mo_2O_5)^{2+}$ Dimer. *Localization of the $(Mo_2O_5)^{2+}$ Dimer.* First, the geometric structures of the $(Mo_2O_5)^{2+}$ dimers grafted on different cluster models were optimized at the BLYP/DNP level and shown in Figure 2. Because of the differences in model size and connectivity to the framework, we cannot directly compare the total energies of different models. So we have to consider the dissociation

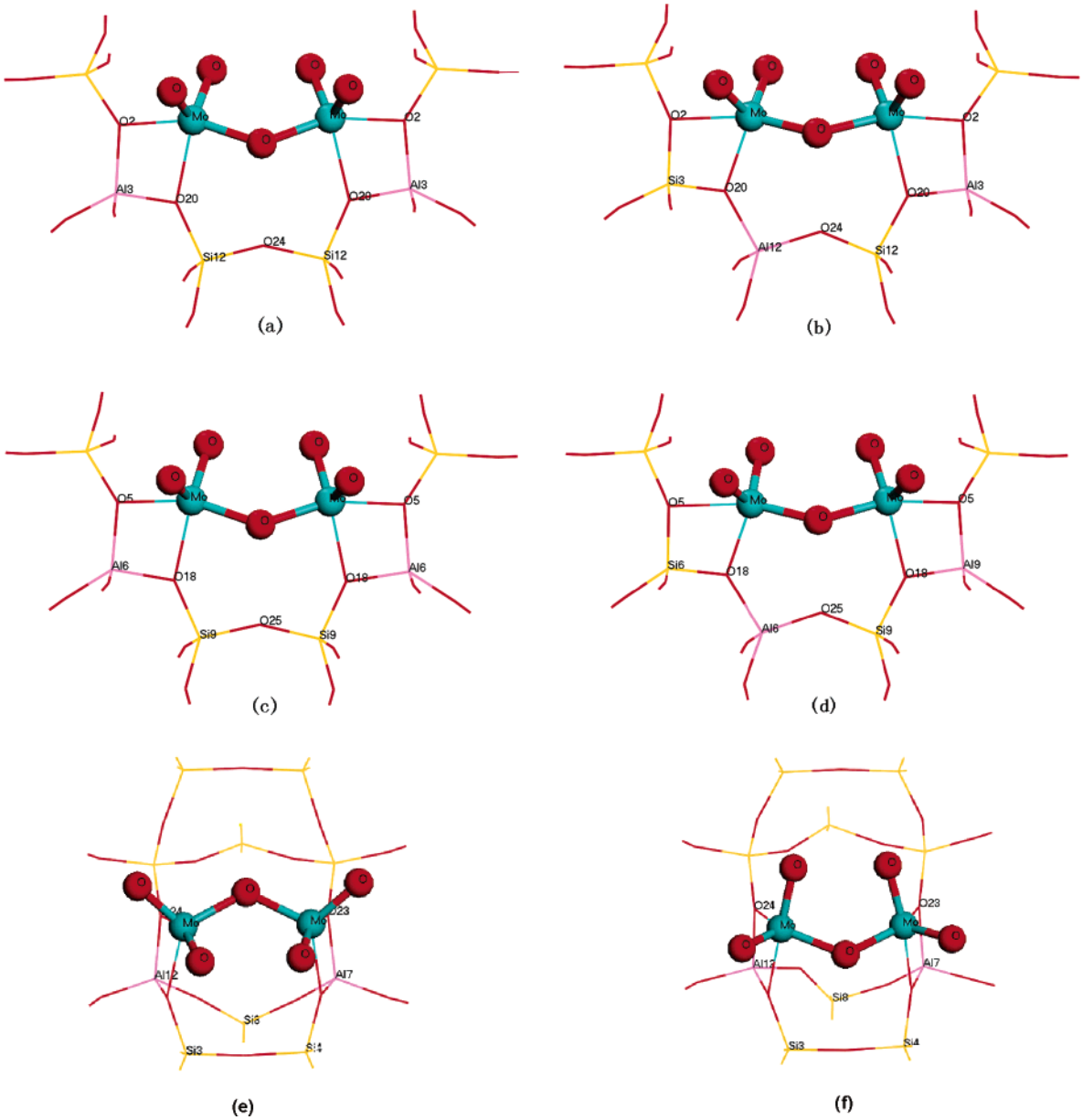

Figure 2. Optimized structures of the $(Mo_2O_5)^{2+}$ dimer grafted at different adjacent B-acid sites on the (a) T3T3 model, (b) T3T12 model, (c) T6T6 model, (d) T6T9 model, (e) T7T12-R model, and (f) T7T12-L model. The terminal hydrogens in all models are veiled for simplicity. The labels correspond to the ZSM5 crystallographic structure.

TABLE 1: Potential Energies and Relative Dissociation Energies of the $Mo_2O_5^{2+}$ Dimer at Different Localizations (Calculated at the BLYP/DNP Level with 6T (or 10T) Cluster Models)

	T6T6	T6T9	T3T3	T3T12	T7T12-R	T7T12-L
E_{tot} (au)	−3595.1398	−3595.1178	−3595.1217	−3595.0989	−4526.7146	−4526.7338
E_D (kcal/mol)	0.38	4.46	(0.00)	2.89	−32.25	−20.21

of the $(Mo_2O_5)^{2+}$ dimer and define the dissociation energy by eq 1

$$Z(Mo_2O_5) \rightarrow Z^{2-} + (Mo_2O_5)^{2+}$$

$$E_D = E(Z^{2-}) - E[Z(Mo_2O_5)] \quad (1)$$

where $E(Z^{2-})$ is the total energy of the optimized cluster model containing two negatively charged Al sites without any charge-compensating counterions and $E[Z(Mo_2O_5)]$ is the total energy of the optimized $(Mo_2O_5)^{2+}$ dimer on different cluster models. To compare the stabilities of different models, we calculated the relative dissociation energies related to the T3T3 model and presented them in Table 1. The dissociation energies of these four models differ by about 3−5 kcal/mol, indicating no apparent difference between their stabilities. For model T7T12, two conformations were obtained and both are obviously unstable. In terms of the preferential localization of framework Al atoms in ZSM5 zeolite, we deduce T6T6 and T6T9 as preferential sittings for the Mo-oxo species, and all discussions in the rest of this paper are related to these two models.

DFT Optimizations with Different Functionals. To examine the dependencies of geometry optimizations on different functionals, we have performed optimizations for the Mo_2O_5/T6T6 model with different methods, and the obtained parameters are shown in Table 2. Comparing with the B3LYP/6-31G** method,

TABLE 2: Geometric Parameters and Energies of the Mo_2O_5/T6T6 Model Calculated with Variable Methods (Bond Length in Å, Bond Angle in Degree)

	PWC	BLYP	PW91	B3LYP	experimental data
Mo≡O	1.712	1.733	1.721	1.703	Mo═O double bond: 1.69 ± 0.008;[12] 1.73;[53]
Mo≡O	1.707	1.732	1.719	1.701	
Mo−Oe	1.887	1.926	1.908	1.909	Mo−O single bond: 1.78 ± 0.0009;[12,53] Mo−O single bond in Mo−O−Mo: 1.84 ± 0.0009;[12,53]
Mo---Mo	3.517	3.570	3.538	3.571	Mo--Mo distance: 3.70 ± 0.0003;[12]
Mo−O_F	2.105	2.158	2.136	2.152	
Mo−O_F	2.156	2.214	2.184	2.191	
Mo--Al	2.977	3.065	3.024	3.052	Mo--Al distance: 3.60 ± 0.0006;[12]
O_F--O_F	4.366	4.340	4.341	4.346	
MoO_FAl	98.2	99.9	99.2	100.3	
MoO_FAl	98.3	99.9	99.2	100.3	
E_{tot} (au)	−3575.7516	−3595.1398	−3595.0855	−3592.8882	

the PWC/DNP method leads to a similar Mo≡O bond length, but Mo−O bonds and Mo−O_F bonds being shorter by about 0.012 Å and 0.047 Å, respectively. Larger discrepancies are related to the Mo−Mo and Mo−Al distances, which are shorter by 0.054 Å and 0.075 Å, respectively. By using BLYP/DNP and PW91/DNP methods, we obtained the reverse results. The Mo≡O bond length becomes longer by about 0.03 Å, and Mo−Mo, Mo−Al distances are merely longer by 0.01−0.03 Å. The results revealed that the local approximation PWC method underestimated the bond lengths, whereas the nonlocal approximation BLYP or PW91 method overestimated the bond lengths. In contrast, the hydride B3LYP/6-31G** method[51,52] gave more reasonable geometries with respect to the reported experimental results.

Characterization of the Geometry of the $(Mo_2O_5)^{2+}$ Dimer. The optimized geometry of the $(Mo_2O_5)^{2+}$ dimer shows a symmetrical feature: four terminal Mo−O bonds are equivalently 1.700 Å long, in good agreement with the experimental data for the distance of the Mo═O double bond.[12,53] The Mo atom connects not only with one framework oxygen atom in the Al−O−Si bridge as other authors indicated[12] but also coordinates concurrently with two oxygen atoms in the O_F−Al−O_F bridge, similar to the localization of other exchanged metallic cations in V/ZSM5, Ga/ZSM5, Cu/ZSM5, and Zn/ZSN5 zeolites.[54−59] The calculated geometries also revealed that each Mo atom bears tetrahedral symmetry. The calculated Mo−O distance in the Mo−O−Mo link is 1.91 Å, matching the experimental data,[12] whereas the Mo−Mo distance is 3.57 Å long, slightly shorter than the experimental data of 3.7 Å. Obvious discrepancies are observed for Mo−Al and Mo−O_F distances. The experimentally determined Mo−Al distance is 3.6 Å; however, the maximal value in our calculated results is 3.20 Å as found in T6T9 mode. Moreover, the calculated Mo−O_F distances are 2.17 Å on average, considerably larger than that of 1.78 Å determined in experiments.[12] With respect to these disagreements, we must keep in mind that X-ray diffraction measures the distance between the electron density centroids, whereas the radial structure functions data obtained by Fourier transform of postedge absorption data (i.e., EXAFS) give distances between neighboring electron clouds. Consequently, the measured data are smaller than the actual interatomic distances between nuclei. However, the experimental data were based on various samples and led to the general results. Recently, Li et al.[53] reported the XRD structural analysis on the structure of Mo-oxo species inside H-ZSM5 zeolite and proposed a $(Mo_5O_{12})^{6+}$ unit situated at the cross point of the straight channel and zigzag channel. That accords for our predictions just as illustrated in Figure 1, where one will notice that all potential Al pair sites capable of taking up an Mo dimer accumulate at the intersections of the zigzag channel and the straight channel. We can propose that the structure of the $(Mo_5O_{12})^{6+}$ units may be an image of the overlapped $(Mo_2O_5)^{2+}$ units. The authors also gave some XRD measured geometric parameters: 1.73 Å for an Mo−O double bond length, 1.78 Å for an Mo−O single bond in the Mo−O−Mo link, and 1.84 Å for an Mo−O single bond, all in good agreement with our calculated results. Figure 3 shows the perspective for the localization of the $(Mo_2O_5)^{2+}$ dimer inside the channel of the ZSM5 zeolite according to our calculations.

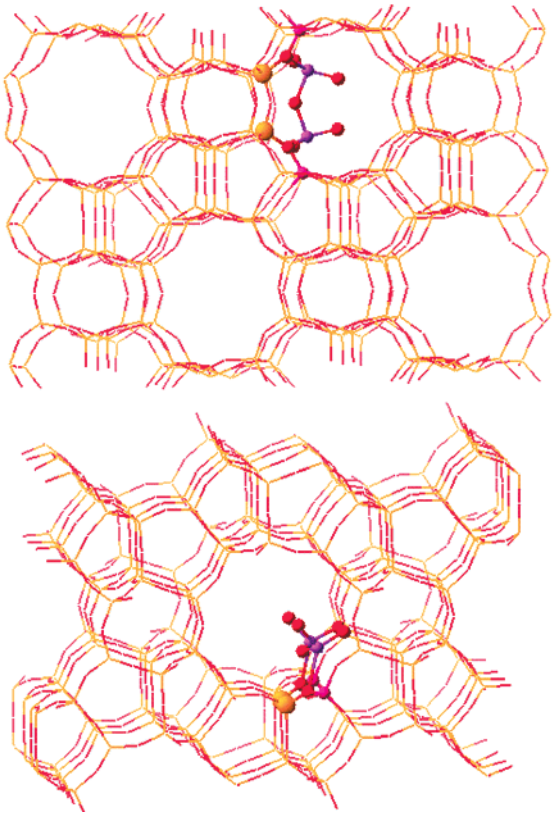

Figure 3. Perspective for the localization of the $(Mo_2O_5)^{2+}$ dimer inside the channel of the ZSM5 zeolite. View in the [100] direction (top) and in the [010] direction (bottom).

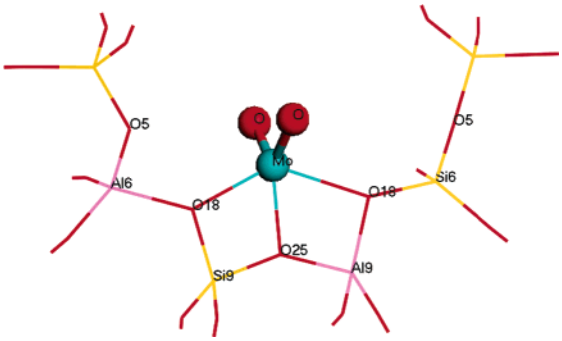

Figure 4. Optimized structure of the $(MoO_2)^{2+}$ monomer grafted at the adjacent B-acid sites on the T6T9 model. The labels correspond to the ZSM5 crystallographic structure.

3.2. Geometric Structure of the $(MoO_2)^{2+}$ Monomer. Many researchers have proposed the Mo monomer as the Mo-oxo species anchored on the zeolite framework.[18,21,25,32] In our previous works,[60,61] we have suggested the $(MoO_2)^{+}$ model to be the monomeric Mo species anchored on one B-acid site, in which the Mo atom is formally charged by +5. In the present work, we explored the $(MoO_2)^{2+}$ model anchored on NNN-positioned B-acid sites with Mo formally charged by +6. We have tested the T6T6 and T6T9 cluster models and confirmed that only the T6T9 model can build a stable $(MoO_2)^{2+}$ monomer. This is because the $(MoO_2)^{2+}$ species must take up two acidic sites, whereas in the T6T6 model the two adjacent B-acid sites are too far to associate $(MoO_2)^{2+}$.

The optimized MoO_2/T6T9 model is shown in Figure 4. The Mo atom bears tetrahedral symmetry and is bridged on Al6−O_F−Si9−O_F−Al9−O_F−Si6; the distances between the Mo and O_F atoms in bridge Al6−O_F−Si9, Si9−O_F−Al9, and Al9−O_F−Si6 are 2.117, 2.005, and 2.372 Å, respectively. Each of the two terminal Mo−O bonds is 1.693 Å long, slightly shorter than that in the $(Mo_2O_5)^{2+}$ dimer. The Mo atom is closer to Al9 with an Mo−Al9 distance of 3.036 Å while more distant to Al6 with 3.733 Å in Mo−Al6. Accidentally, this parameter is in better agreement with the experimentally determined Mo−Al distance of 3.6 Å.[12] Except for the discrepancies between experimental determination and theoretical calculation, it reveals the fact that in the actual samples the Mo monomer and Mo dimer may coexist.

3.3. Raman Vibrational Frequencies for the $(Mo_2O_5)^{2+}$ Dimer and the $(MoO_2)^{2+}$ Monomer. The vibrational frequency of the $(Mo_2O_5)^{2+}$ dimer for Raman-active mode was calculated using the DFT method. Table 3 lists the frequencies and the corresponding vibrational modes as well as the experimental data in references. We found a stretching mode for terminal Mo≡O at 970 cm^{-1} and the stretching for O≡Mo≡O at 983 cm^{-1} (symmetric) and 955 cm^{-1} (asymmetric), which match very well to the Raman spectra in the experiments by Iglesia's group.[12] In their results, however, the strong vibrational bands around 400 and 1000 cm^{-1} were not explained satisfactorily. In our simulated spectrum, the vibrations of Mo−O−Mo bending gave bands at 328 and 473 cm^{-1}, which are obviously higher than that experimentally observed at 300 cm^{-1} for isolated MoO_x,[12] just attributed to the constrained Mo_2O_5 structure grafted on the frameworks. The bands at 346 and 365 cm^{-1} are related to the bending of O≡Mo≡O, and the bands ranging from 405 to 447 cm^{-1} are related to the stretching modes between Mo and the framework oxygens. The bands from 995 to 1055 cm^{-1} are ascribed to the stretching of O≡Mo≡O accompanied with strong stretching vibrations of framework O_F−Al−O_F, which mimic the experimentally detected frequency at 1045 cm^{-1}. These results provide the evidence that the MoO_x species associated with frameworks lead to higher frequencies of Mo≡O stretching. Our calculated frequencies based on the optimized model agree well with the experiments. For the $(MoO_2)^{2+}$ monomer, O≡Mo≡O symmetric stretching was observed at 995 and 1011 cm^{-1}, accompanied by strong vibrations of frameworks. No isolated O≡Mo≡O symmetric stretching was found; just an asymmetric stretching was at 972 cm^{-1}, which is higher than that in the Mo dimer, corresponding to the shorter Mo≡O bond in the Mo monomer. These results prove that the $(MoO_2)^{2+}$ monomer is more tightly connected with the frameworks.

TABLE 3: Raman Vibrational Frequencies (cm^{-1}) Calculated for the Mo_2O_5/T6T6 Model and the MoO_2/T6T9 Model (Corrected with a Scaling Factor of 0.96) and from the Experiments[a]

vibrational mode	frequency from calculation		frequency from experiment (ref 12)
	Mo_2O_5/T6T6	MoO_2/T6T9	
stretching			
ν_s Mo≡O	970		1000 (960)
ν_s O≡Mo≡O	983		
ν_{as} O≡Mo≡O	947, 955	972	
ν_s O≡Mo≡O	995, 1003, 1022, 1055	995, 1011	970, 1045
and			
ν_s O_F−Al−O_F			
ν_s Mo−O−Mo	761		(820)
ν Mo−O_F	405, 430, 447	492, 535, 590	
bending			
ρ Mo−O−Mo	328, 473		
ρ O≡Mo≡O	346, 365	326, 354, 361	(300)

[a] The frequencies presented in parentheses are attributed to the vibrations in bulk MoO_3 crystallites (ref 12 and references therein).

3.4. Electronic Structure Analysis by NBO Calculations. *$(Mo_2O_5)^{2+}$Dimer.* According to the natural population analysis for the $(Mo_2O_5)^{2+}$ dimer, we find the natural charges of +1.92*e* on Mo atom and its effective valence electronic configuration is represented as 5s(0.20)4d(3.85). Obviously, the lost two electrons come separately from 5s and 4d orbitals. Four valence electrons distribute equivalently in five 4d orbitals. The binding information for the $(Mo_2O_5)^{2+}$ dimer was given by NBO analysis and demonstrated in Table 4. One observes a triple bond between Mo and the terminal oxygen. The NBO plots of BD(1), BD(2), and BD(3) (stand for single, double, and triple bonds of Mo−O) are shown in Figure 5d−f, respectively. In the Mo_2O_5 unit, three Mo≡O triple bonds and one Mo═O double bond are found. In the Mo−O−Mo link, Mo and O atoms are connected through a σ bond. A single bond also exists between Mo and the framework oxygen O_F (its plot is shown in Figure 5g). In the T6T6 model, just three single Mo−O_F bonds are observed and one is absent. The corresponding binding relates to the σ-donation of the p orbital of O_F to the Mo−O antibond, which will be discussed later. From Table 4, one can find that all single, double, and triple bonds have the deficient electron occupancies, whereas in the corresponding antibonding orbitals excessive electrons exist, implying the existence of a conjugated orbital system. To get the information on bond−bond interactions in the overall system, we carried out the second-order perturbation theory analysis for NBOs and the selected data are shown in Table 5. Because the Mo dimer takes a symmetrical structure, for simplicity, only parts of the data are demonstrated.

As mentioned above, no bond was observed between Mo and framework oxygen O18; instead, we find strong σ-donation from

TABLE 4: NBO Analysis for the Mo_2O_5/T6T6 Model: Natural Bond Orbitals and Occupancy

NBO valence bond	occupancy	coefficient/hybrids	NBO antibond	occupancy	bond type
BD(1)Mo1−Oa[a]	1.823	$0.393(sp^{1.3}d^{6.3})_{Mo} + 0.919(sp^{8.6})_O$	BD*(1)Mo1−Oa[a]	0.182	Mo≡O triple bonds
BD(2)Mo1−Oa	1.901	$0.454(sd^{4.0})_{Mo} + 0.891\ (p)_O$	BD*(2)Mo1−Oa	0.223	
BD(3)Mo1−Oa	1.898	$0.538\ (d)_{Mo} + 0.843\ (p)_O$	BD*(3)Mo1−Oa	0.171	
BD(1)Mo1−Ob	1.886	$0.471\ (sd^{3.3})_{Mo} + 0.882\ (sp^{4.7})_O$	BD*(1)Mo1−Ob	0.132	
BD(2)Mo1−Ob	1.836	$0.394\ (d)_{Mo} + 0.919\ (p)_O$	BD*(2)Mo1−Ob	0.249	
BD(3)Mo1−Ob	1.884	$0.511\ (d)_{Mo} + 0.860\ (p)_O$	BD*(3)Mo1−Ob	0.211	
BD(1)Mo2−Oc	1.941	$0.476\ (sd^{7.9})_{Mo} + 0.880\ (sp^{8.6})_O$	BD*(1)Mo2−Oc	0.299	
BD(2)Mo2−Oc	1.798	$0.387\ (d)_{Mo} + 0.922\ (p)_O$	BD*(2)Mo2−Oc	0.177	
BD(3)Mo2−Oc	1.893	$0.536\ (d)_{Mo} + 0.844\ (p)_O$	BD*(3)Mo2−Oc	0.169	
BD(1)Mo2−Od	1.887	$0.472(sd^{4.1})_{Mo} + 0.882\ (sp^{4.7})_O$	BD*(1)Mo2−Od	0.143	Mo═O double bond
BD(2)Mo2−Od	1.881	$0.509(d)_{Mo} + 0.861\ (p)_O$	BD*(2)Mo2−Od	0.209	
BD(1)Mo1−Oe	1.875	$0.950\ (sp)_O + 0.313\ (sp^{1.2}d^{2.7})_{Mo}$	BD*(1)Mo1−Oe	0.189	Mo−O−Mo link
BD(1)Mo2−Oe	1.874	$0.312\ (sp^{1.1}d^{2.2})_{Mo} + 0.950\ (sp)_O$	BD*(1)Mo2−Oe	0.184	
BD(1)Mo2−O5	1.889	$0.268\ (sp^{1.3}d^{2.7})_{Mo} + 0.964\ (sp^{2.7})_O$	BD*(1)Mo2−O5	0.271	Mo−O_F single bonds
BD(1)Mo2−O18′	1.898	$0.252\ (sd^{2.4})_{Mo} + 0.968\ (sp^{2.7})_O$	BD*(1)Mo2−O18′	0.313	
BD(1)Mo1−O5	1.890	$0.269\ (sp^{1.1}d^{2.4})_{Mo} + 0.963\ (sp^{2.7})_O$	BD*(1)Mo2−O5	0.268	
LP(1)O18[b]	1.794				

[a] BD(1), BD(2), and BD(3) denote single bond, double bond, and triple bond, respectively; BD* denotes the corresponding antibonds. [b] LP denotes the lone pair.

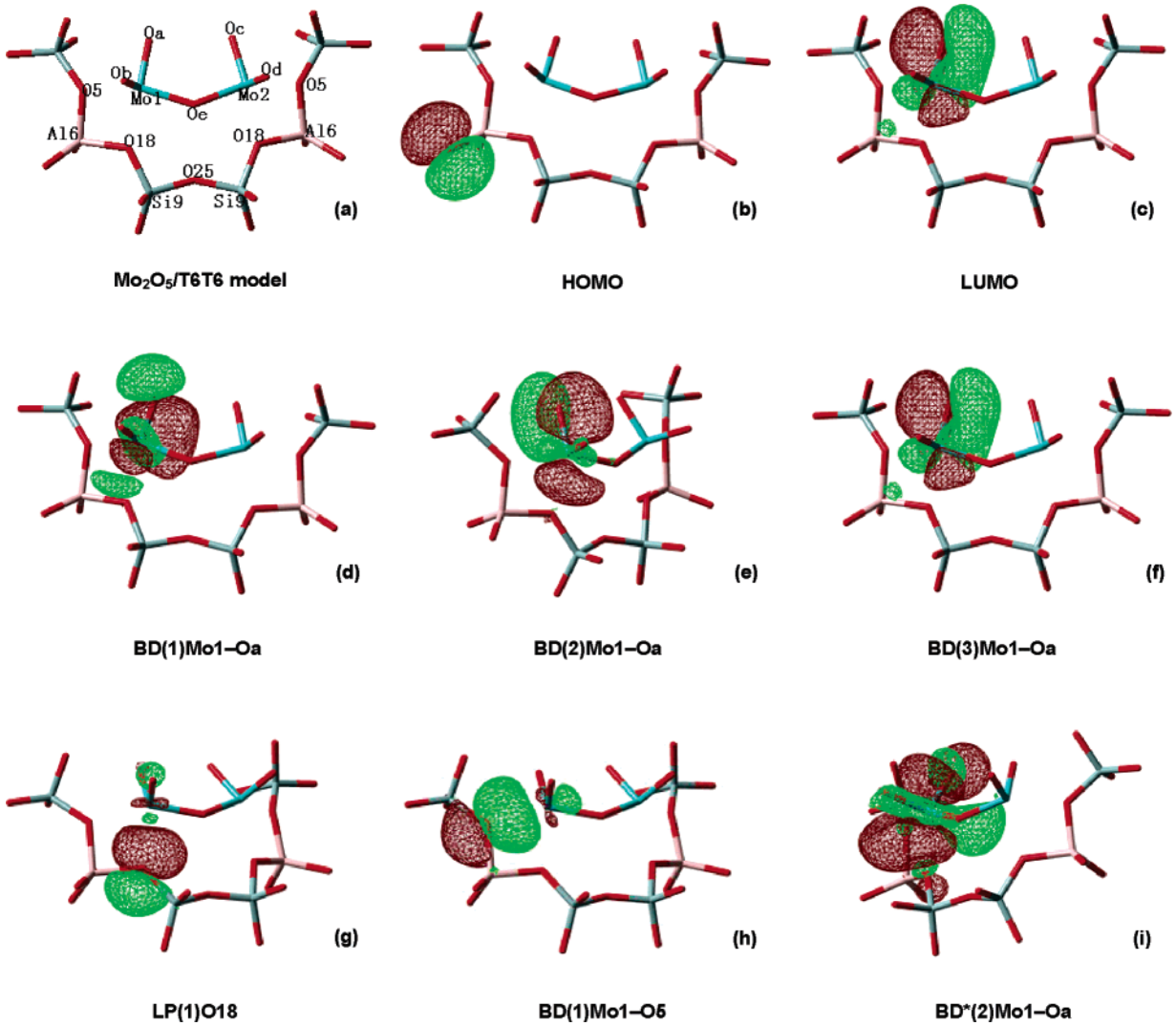

Figure 5. NBO plots for molecular orbitals in the Mo_2O_5/T6T6 model: (a) Mo_2O_5/T6T6 model showing labeling; (b) HOMO; (c) LUMO; (d) Mo−O single bond; (e) Mo−O double bond; (f) Mo−O triple bond; (g) Mo−OF bond; (h) donation from OF to Mo; (i) Mo−O double antibond.

the p orbital in O18 to the π^* orbital in the Mo1−Oa bond (see plots in Figure 5h and i). In fact, other σ orbitals in the Mo−O_F bond are strongly polarized toward the O_F atom. For instance, the NBO hybrid orbital in Mo1−O5 is constructed of 0.269 $(spd^{2.4})_{Mo} + 0.963\ (sp^{2.8})_O$; the electron density in this single bond is 92.79% polarized at O5 (see plot in Figure 5g). The NBO plots of these two orbitals look identical. In addition, in the non-framework Mo_2O_5 unit, one finds the electron trans-

TABLE 5: Second-Order Perturbation Stabilization Energies $\Delta E(2)$ for the Mo_2O_5/T6T6 Model

donor NBO	acceptor NBO	$\Delta E(2)$/kcal/mol	type of interaction
BD(1)Mo1−Oa[a]	BD*(2)Mo1−Ob[a]	73.6	Mo_2O_5 conjugate
BD(2)Mo1−Oa	BD*(1)Mo1−Ob	65.7	conjugated O≡Mo≡O
BD(3)Mo1−Oa	BD*(3)Mo1−Ob	42.2	
BD(1)Mo1−Ob	BD*(2)Mo1−Oa	49.1	
BD(2)Mo1−Ob	BD*(1)Mo1−Oa	24.3	
BD(3)Mo1−Ob	BD*(3)Mo1−Oa	18.8	
BD*(3)Mo1−Oa	BD*(3)Mo1−Ob	46.5	
LP(2)Od[b]	BD*(1)Mo2−Oc	30.8	O: → Mo−O
LP(2)Od	BD*(1)Mo2−O18′	26.1	
BD(2)Mo1−Oa	BD*(1)Mo1−Oe	25.1	Mo_2O_5 → O−Mo−O conjugated bond
BD(3)Mo1−Oa	BD*(1)Mo1−Oe	19.9	
BD(1)Mo1−Ob	BD*(1)Mo1−Oe	22.4	
BD(3)Mo1−Ob	BD*(1)Mo1−Oe	35.7	
BD(1) Mo1−O5	BD*(3)Mo1−Oa	11.6	O_F−Mo → Mo_2O_5 conjugated bond
BD(3)Mo1−Oa	BD*(1)Mo1−O5	24.4	
BD*(3)Mo1−Oa	BD*(1)Mo1−O5	31.1	
BD*(1)Mo1−O5	BD*(2)Mo1−Oa	30.3	
BD(1)Mo1−O5	BD*(3)Mo1−Ob	18.1	
BD(3)Mo1−Ob	BD*(1)Mo1−O5	26.2	
BD*(1)Mo1−O5	BD*(2)Mo1−Ob	31.6	
BD*(1)Mo1−O5	BD*(1)Mo1−Ob	19.6	
BD*(3)Mo1−Oa	BD*(1)Mo1−O5	31.1	
BD(3)Mo1−Oa	BD*(1)Mo1−O5	24.4	
LP(1)O18	BD*(2)Mo1−Oa	47.8	O_F → Mo
LP(1)O18	BD*(2)Mo1−Ob	20.6	
BD(1) Mo1−O5	BD*(1)Mo1−Oe	21.4	O_F−Mo → O−Mo−O (O5−Mo−Oe) conjugate
BD(1)Mo1−Oe	BD*(1)Mo1−O5	35.4	

[a] BD(1), BD(2), and BD(3) denote single bond, double bond, and triple bond, respectively; BD* denotes the corresponding antibonds. [b] LP denotes the lone pair.

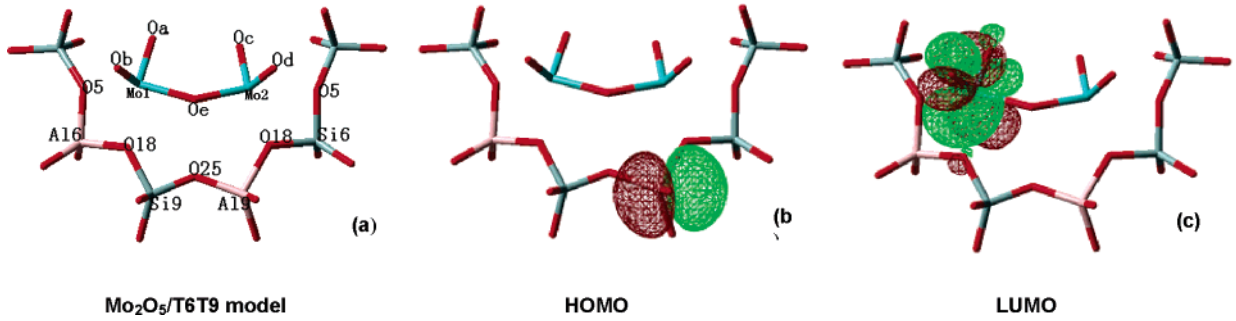

Figure 6. NBO plots for molecular orbitals in the Mo_2O_5/T6T9 cluster model: (a) Mo_2O_5/T6T9 model showing the labels; (b) HOMO; (c) LUMO.

formation from occupied σ and π orbitals to σ^* and π^* orbitals as well as electron transformation between σ^* and π^* orbitals, implying the existence of an expanded electron conjugation system that further extends to framework O_F−Al−O_F bridges. Five of the 4d orbitals in the Mo atom contribute to binding with oxygens; no vacant d orbital or nonbonding single d electron remains among the valence orbitals of the Mo atom. The HOMO in the $(Mo_2O_5)^{2+}$ dimer is related to the p orbital of the framework oxygen (Figure 5b), whereas the LUMO is attributed to BD*(3)Mo1−Oa, that is, the π^* orbital of the Mo≡Oa triple bond (Figure 5c). In fact, the LUMO is a conjugated antibonding orbital system, which can be determined through the strong stabilization for the interaction between BD*(3)Mo1−Oa and BD*(3)Mo1−Ob orbitals. That means that the $(Mo_2O_5)^{2+}$ species would provide its conjugated antibonding π orbitals as a nucleophilic attacking center during catalytic reactions. This is crucial for the reduction and carburetion by the methane molecule to form molybdenum carbide. The reactivity of the $(Mo_2O_5)^{2+}$ dimer will be discussed in Section 3.6. For the Mo_2O_5/T6T9 model, the frontier molecular orbital configurations are similar to those of the T6T6 model (Figure 6).

$(MoO_2)^{2+}$ Monomer. According to the natural population analysis for the $(MoO_2)^{2+}$ monomer, we find the natural charges of $+2.07e$ on the Mo atom, slightly higher than that in the Mo dimer, and its effective valence electronic configuration is represented as 5s(0.17)4d(3.75). Five 4d orbitals are equivalently occupied. The binding characteristic for the $(MoO_2)^{2+}$ monomer was examined by NBO analysis and demonstrated in Tables 6 and 7. We find triple bonds in terminal Mo−Oa and Mo−Ob, equivalent to the bond type in the $(Mo_2O_5)^{2+}$ dimer. A single bond is observed between the Mo atom and framework oxygen O18′. Simultaneously, there are the interactions between the Mo atom and framework oxygen O25 and O18, contributed by the electron donation from the sp^3 long pair orbital in O25 to π^* of Mo−Ob, and from the sp^3 long pair orbital in O18 to σ^* of Mo−O18′ as well as to π^* of Mo−Oa and Mo−Ob. There are also conjugated π orbitals in the O≡Mo≡O system that even extended to framework oxygens. The HOMO in the $(MoO_2)^{2+}$

TABLE 6: NBO Analysis for the $(MoO_2)^{2+}$ Monomer on T6T9: Natural Bond Orbitals and Occupancy

NBO valence bond	occupancy	NBO antibond	occupancy	bond type
BD(1)Mo−Oa[a]	1.924	BD*(1)Mo−Oa[a]	0.148	Mo═O
BD(2)Mo−Oa	1.972	BD*(2)Mo−Oa	0.196	double bond
BD(1)Mo−Ob	1.953	BD*(1)Mo−Ob	0.175	and Mo≡O
BD(2)Mo−Ob	1.978	BD*(2)Mo−Ob	0.199	triple bond
BD(3)Mo−Ob	1.951	BD*(3)Mo−Ob	0.401	
LP(1)O25[b]	1.731			long pair
LP(1)O18	1.868			p electrons
LP(2)O18	1.713			
LP(2)Oa	1.619			

[a] BD(1), BD(2), and BD(3) denote single bond, double bond, and triple bond, respectively; BD* denotes the corresponding antibond.[b] LP denotes the lone pair.

TABLE 7: Second-Order Perturbation Stabilization Energies $\Delta E(2)$ for the MoO_2/T6T9 Model

donor NBO (i)	acceptor NBO (j)	$\Delta E(2)$/ kcal/mol	type of interaction
BD(1)Mo−Oa[a]	BD*(1)Mo−Oa[a]	15.8	conjugated O≡Mo≡O
BD(1)Mo−Oa	BD*(1)Mo−Ob	24.4	
BD(1)Mo−Oa	BD*(3)Mo−Ob	15.9	
BD(1)Mo−Ob	BD*(1)Mo−Oa	20.5	
BD(1)Mo−Ob	BD*(1)Mo−Ob	11.1	
BD(3)Mo−Ob	BD*(1)Mo−Oa	19.5	
BD(3)Mo−Ob	BD*(1)Mo−Ob	10.1	
BD(1)Mo−O18′	BD*(1)Mo−Oa	15.2	
BD(1)Mo−O18′	BD*(1)Mo−Ob	13.6	
BD(1)Mo−Ob	BD*(1)Mo−O18′	16.9	O≡Mo≡O → Mo−O_F
LP(2)Oa[b]	BD*(1)Mo−Ob	12.5	O: → Mo−O
LP(2)Oa	BD*(3)Mo−Ob	39.8	
LP(1)O25	BD*(1)Mo−Oa	19.2	O_F → O≡Mo≡O
LP(1)O25	BD*(2)Mo−Ob	20.7	
LP(1)O25	BD*(3)Mo−Ob	66.6	
LP(2)O18	BD*(1)Mo−Oa	19.1	
LP(2)O18	BD*(2)Mo−Ob	11.1	
LP(2)O18	BD*(3)Mo−Ob	17.1	
LP(2)O18	BD*(1)Mo−O18′	39.8	O_F → Mo−O_F
BD*(1)Mo−Oa	BD*(1)Mo−Oa	235.7	
BD*(3)Mo−Ob	BD*(1)Mo−O18′	30.5	
BD*(1)Mo−O18′	BD*(1)Mo−Oa	114.9	
BD*(1)Mo−O18'	BD*(1)Mo−Ob	146.9	

[a] BD(1), BD(2), and BD(3) denote single bond, double bond, and triple bond, respectively; BD* denotes the corresponding antibond.[b] LP denotes the lone pair.

monomer is attributed to the p orbital in a framework oxygen, whereas LUMO is assigned to π^* of Mo−Oa double bond. Consequently, the $(MoO_2)^{2+}$ monomer is capable of being reduced by the methane molecule. The NBO plots are shown in Figure 7.

3.5. Formation of $(Mo_2O_5)^{2+}$/ZSM-5 and $(MoO_2)^{2+}$/ZSM-5. As proposed by Iglesia and co-workers,[12,27,30] the exchanged Mo species anchored on the framework as an isolated $(Mo_2O_5)^{2+}$ dimer associated with two Al sites (Scheme 1):

Because the isolated MoO_3 species are too large to migrate into the zeolite channels, the practical reactive Mo species may be $MoO_2(OH)_2$ as proposed by other authors[27] and by our previous calculation.[17] Therefore, it is worthwhile to consider the stepwise reactions

$$Z{-}H_2 + MoO_2(OH)_2 \rightarrow Z{-}H_2\,MoO_2(OH)_2 \quad \Delta E_{1a}$$

$$Z{-}H_2\,MoO_2(OH)_2 \rightarrow Z{-}HMoO_2(OH) + H_2O \quad \Delta E_{1b}$$

$$Z{-}HMoO_2(OH) + MoO_2(OH)_2 \rightarrow Z{-}HMoO_2(OH)\,MoO_2(OH)_2 \quad \Delta E_{2a}$$

$$Z{-}HMoO_2(OH)\,MoO_2(OH)_2 \rightarrow Z(MoO_2(OH))_2 + H_2O \quad \Delta E_{2b}$$

$$Z(MoO_2(OH))_2 \rightarrow Z(Mo_2O_5) + H_2O \quad \Delta E_3$$

$$Z{-}H\,MoO_2(OH) \rightarrow Z(MoO_2) + H_2O \quad \Delta E_4$$

$$\Delta E_{1a} = E[Z{-}H_2\,MoO_2(OH)_2] - E[Z{-}H_2] - E[MoO_2(OH)_2]$$

$$\Delta E_{1b} = E[Z{-}HMoO_2(OH)] + E[H_2O] - E[Z{-}H_2\,MoO_2(OH)_2]$$

$$\Delta E_{2a} = E[Z{-}HMoO_2(OH)\,MoO_2(OH)_2] - E[Z{-}HMoO_2(OH)] - E[MoO_2(OH)_2]$$

$$\Delta E_{2b} = E[Z(MoO_2(OH))_2] + E[H_2O] - E[Z{-}HMoO_2(OH)\,MoO_2(OH)_2]$$

$$\Delta E_1 = \Delta E_{1a} + \Delta E_{1b}$$

$$\Delta E_2 = \Delta E_{2a} + \Delta E_{2b}$$

$$\Delta E_3 = E[Z(Mo_2O_5)] + E[H_2O] - E[Z(MoO_2(OH))_2]$$

$$\Delta E_4 = E[Z(MoO_2)] + E[H_2O] - E[Z{-}H\,MoO_2(OH)]$$

where in our case $Z{-}H_2$ represents the double Al substituted zeolite model (T6T6 or T6T9); $Z{-}H_2MoO_2(OH)_2$ and $Z{-}HMoO_2(OH)MoO_2(OH)_2$ represent the adsorption complexes; $Z{-}H(MoO_2(OH)$ and $Z(MoO_2(OH))_2$, respectively, represent one- and two-Mo loaded zeolite models; and $Z(Mo_2O_5)$ and $Z(MoO_2)$ stand for the $(Mo_2O_5)^{2+}$ dimer and $(MoO_2)^{2+}$ monomer, respectively. In the first step of the processes, the $MoO_2(OH)_2$ molecule attacks the B-acid site to form an adsorption complex, which then associates with the B-acid, producing the loaded Mo species. The formation of the Mo dimer goes through Step 1, Step 2, and Step 3, while Mo monomer undergoes Step 1 and Step 4. The corresponding reaction energies for the stepwise reactions were calculated and listed in Table 8.

First, we have to take into account the stability and acidity of the $Z{-}H_2$ model. Although a number of theoretical studies have been made on the stabilities and the acid strength of adjacent B-acid sites in zeolites,[61−66] some reversed results were obtained; the dependency of Si/Al substitution on the acid strength were not uniform and correlated to the location of referent Al and the proton position.[65,66] The drawn conclusions varied with the type of investigated zeolites.[62,63,65] For the T6T6 model, which belongs to the NNNN-acid site, there are three cases for the localizations of protons as T6(H)T6(H), T6(H)(H)T6, and (H)T6T6(H), in which the T6(H)T6(H) form was verified by theoretical calculations to have better stability and stronger acidity. For the T6T9 model, which belongs to the NNN-acid site, the favorable locations of protons is the T6(H)T9(H) form. In our present work, the $Z{-}H_2$ is taken as the T6(H)T6(H) or T6(H)T9(H) form.

On the T6T6 model, only the $(Mo_2O_5)^{2+}$ dimer was obtained; no stable conformation of the $(MoO_2)^{2+}$ monomer was found because the distance between two B-acid sites is too long to build such a dinetate complex. The replacement of the first acidic

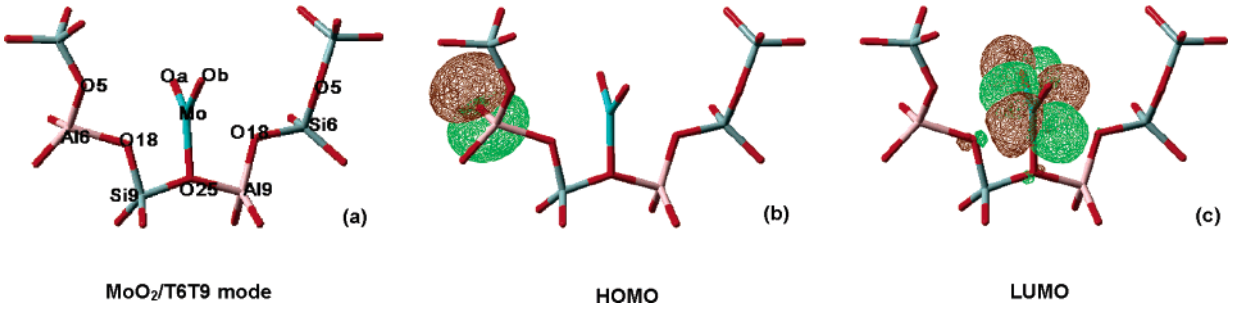

Figure 7. NBO plots for molecular orbitals in the MoO_2/T6T9 model: (a) MoO_2/T6T9 model showing the labels; (b) HOMO; (c) LUMO.

SCHEME 1

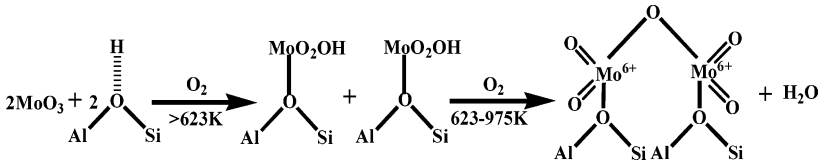

SCHEME 2: Proposed Mo Monomer and Dimer Structures and Formation Processes

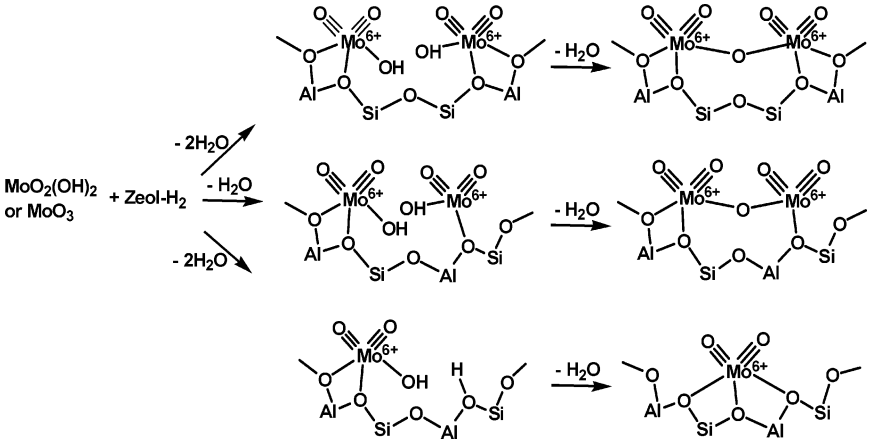

TABLE 8: Stepwise Reaction Energies for the Formation of the $(Mo_2O_5)^{2+}$ Dimer and the $(MoO_2)^{2+}$ Monomer (kcal/mol)

	Mo_2O_5/T6T6	Mo_2O_5/T6T9	MoO_2/T6T9
ΔE_{1a}	−16.35	−4.25	−4.25
ΔE_{1b}	19.51	15.62	15.62
ΔE_1	3.16	11.38	11.38
ΔE_{2a}	−21.96	−15.92	
ΔE_{2b}	21.49	10.47	
ΔE_2	−0.47	−5.45	
ΔE_3	−2.83	9.19	
ΔE_4			37.74
ΔE_{tot}	−0.14	15.12	49.12

proton of T6T6 by a $MoO_2(OH)_2$ molecule is an endothermic process (ΔE_1), whereas the followed replacement of second acidic proton is slightly exothermic (ΔE_2). The condensation of two adjacent $-MoO_2(OH)$ species is also exothermic (ΔE_3). For the T6T9 model, we have obtained stable conformations of the $(Mo_2O_5)^{2+}$ dimer and the $(MoO_2)^{2+}$ monomer. The loading of the first Mo is more difficult than that in T6T6 because the acidity of NNN-sites is weaker than that of NNNN-sites. Nevertheless, the loading of the second $MoO_2(OH)_2$ is energetically favorable. Although the first loaded $-MoO_2(OH)$ moiety would hinder the neighboring B-acid site from the attack of another $MoO_2(OH)_2$ molecule, the loaded two $-MoO_2(OH)$ moieties are so close that multiple hydrogen bonds are formed between them and between the framework oxygens and the $-MoO_2(OH)$ moieties; consequently, the calculated formation energies in Step 2 are lower. The condensation of two adjacent $-MoO_2(OH)$ species in the T6T9 model is endothermic, indicating that the Mo_2O_5/T6T9 model is less favorable to build because its structure has to bear stronger strain. If no second Mo was loaded on the NNN-acid site, then the $-MoO_2OH$ moiety could associate with the adjacent Brönsted acidic proton to form the $(MoO_2)^{2+}$ monomer. This species is coordinated with three framework oxygens as shown in Figure 4, and its conformation is further strained; consequently, one finds a greater formation energy for the MoO_2/T6T9 model.

From the optimized adsorption complexes, we find that the $MoO_2(OH)_2$ molecule is adsorbed on the B-acid site through hydrogen bonding; the calculated adsorption energies range from −5 to −22 kcal/mol, implying that the adsorption complexes may not stably exist at the experimental temperatures up to 773 K. Although the preference for Mo oxo formation decreases as Mo_2O_5/T6T6 > Mo_2O_5/T6T9 > MoO_2/T6T9, in the view of thermodynamics they are all able to build at the experimental temperatures up to 973 K. The final Mo species anchored in the channels of HZSM-5 depend on the Si/Al ratio and the amount of Mo loading.[32] When Si/Al = 40 and Mo loading is 2 wt %, corresponding to an Mo/Al ratio of 0.2, the probability of two adjacent B-acid sites in NNNN-sites is higher than that in NNN-sites, so the only anchored Mo oxo species should be the $(Mo_2O_5)^{2+}$ dimer and prefer to locate at NNNN-sites. This accords with the experimental results reported by different groups.[27,32,35] When Si/Al = 15 and Mo loading is 2 wt %,

corresponding to an Mo/Al ratio of 0.5, the probability of NNN-sites increases, but the Mo loading is not enough for full occupation of NNN-acid sites. That means that some single $MoO_2(OH)$ moieties exist on NNN-sites, which have to be associated with nearest-neighboring B-acid sites to form $(MoO_2)^{2+}$ monomers, as proposed by Louis.[32] The proposed formation pathways for the $(Mo_2O_5)^{2+}$ dimer and the $(MoO_2)^{2+}$ monomer are demonstrated in Scheme 2. There the bonding characteristics of the $(Mo_2O_5)^{2+}$ dimer and the $(MoO_2)^{2+}$ monomer are also illustrated.

3.6. Activity for Methane C−H Bond Dissociation. The Mo-oxo species are the stable products in the preparation of the Mo/H-ZSM5 catalyst. During initial contact of MoO_x/H-ZSM5 with gas-phase methane at 950 K, the MoO_x species can be reduced and carburized to form the MoC_x species by delivering predominant products of CO, CO_2, H_2O, and H_2.[25] In the present paper, we are interested in the mechanism of the Mo dimer for methane activation and examine the reactivity of the optimized $(Mo_2O_5)^{2+}$ model toward the C−H bond dissociation of methane. The NBO analysis on the $(Mo_2O_5)^{2+}$ dimer indicated that the HOMO is related to the p orbital in the framework oxygen and the LUMO is attributed to the antibonding π-orbital in the terminal Mo−O bond. Consequently, the $(Mo_2O_5)^{2+}$ dimer behaves as the electron-deficient active center. The reaction of methane on the $(Mo_2O_5)^{2+}$ dimer would occur between the LUMO of the Mo dimer and the HOMO of methane. The LUMO energy in the Mo dimer system is 7.8 eV higher than the HOMO of methane. Using DFT calculations, we identified the transition state of methane C−H bond dissociation on the Mo dimer with only one imaginary frequency at -1230 cm^{-1} with H stretching between the O atom in Mo1≡Oa and the C atom in CH_4. The stationary distance between C and H was 1.617 Å, the Mo−C distance was 2.488 Å, and the H−O distance was 1.118 Å. The corresponding activation energy was 63.5 kcal/mol. After the cleavage of the C−H bond, the methyl moiety was bonded to the Mo atom and the H atom was transferred to the oxygen of the Mo≡Oa group. The total energy of the dissociated system was 38 kcal/mol over the reactant system. In our previous work, a similar process for C−H bond dissociation on $(MoO_2)^+$/ZSM5 led to an activation energy of 38 kcal/mol.[67] The results suggest that the C−H bond dissociation on the Mo(VI) center has to overcome a higher energy barrier than that on the Mo(V) center. Fu et al.[68] have reported the computational studies on methane C−H bond activation on the isolated Mo_3O_9 cluster and obtained the activation energy of 63 kcal/mol for the same pathway using the (O═Mo−O−Mo═O) unit as the active center. In their report, the same pathway on the single Mo═O active center gave an activation energy of 87 kcal/mol. Therefore, it can be proposed that the conjugated π*-orbital system plays a central role in reducing the energy barrier on the methane oxidation.

4. Conclusions

The geometric structures of the $(Mo_2O_5)^{2+}$ dimer and the $(MoO_2)^{2+}$ monomer grafted on the framework of the ZSM5 zeolite were optimized using the DFT approach. The hydride B3LYP method led to more reasonable results. The stabilities of the $(Mo_2O_5)^{2+}$ dimers located at the T3T3, T6T6, T6T9, and T3T12 sites are generally equivalent. The $(Mo_2O_5)^{2+}$ dimer located at the NNNN-site shows good structural symmetry, with each Mo atom coordinated with two framework bridging oxygen atoms on the O_F-Al-O_F bridge. The calculated distances of terminal Mo−O double or triple bonds are about 1.70 Å (experimental data of 1.73 Å), the Mo−O distance in the Mo−O−Mo link is 1.91 Å (experimental data of 1.84 Å), and the distances between Mo and framework oxygen O_F are 2.17 Å on average, which match mostly with the experimental results. The calculated Raman vibrational frequencies at 995 and 1055 cm^{-1} are attributed to the O≡Mo≡O stretching accompanied with the strong vibrations of the framework, which are in good agreement with the experimental result.

Natural bond orbital (NBO) analysis provided binding characteristics on the $(Mo_2O_5)^{2+}$ dimer and the $(MoO_2)^{2+}$ monomer. It was confirmed that the terminal Mo−O bonds are triple bonds, and the Mo atoms are coordinated with the framework oxygens in bridge O_F-Al-O_F through σ donations of the p orbital in O_F to antibonded orbitals in Mo−O bonds. In MoO_2 and the Mo_2O_5 unit there are conjugated π-electronic systems that further extend to the frameworks. NBO analysis revealed that the HOMO in the $(Mo_2O_5)^{2+}$ dimer is the p orbital in a framework oxygen and the LUMO is the π* orbital in the Mo≡O triple bond. The formations of the Mo monomer and dimer were examined by calculating the stepwise reaction energies. It was concluded that the $(Mo_2O_5)^{2+}$ dimer is more preferred to form at NNNN-acidic sites than at NNN-acidic sites; the $(MoO_2)^{2+}$ monomer can only be formed at NNN-acidic sites, and the formation energy is higher than that of the dimer. Finally, we examined the activity of the $(Mo_2O_5)^{2+}$ dimer for methane C−H bond dissociation. In the transition state, methane approaches the Mo≡O group with the methyl group attacking the metal and H attacking the oxygen. The activation energy was obtained to be 63.5 kcal/mol.

Acknowledgment. We are grateful to the Education Ministry of Liaoning Province (A:205L211) and Liaoning Normal University for financial support. We also acknowledge Prof. X.H. Bao's group in the State Key Laboratory of Catalysis, Dalian Institute of Chemical Physics for the extended scientific cooperation.

Supporting Information Available: The geometric parameters of the $(Mo_2O_5)^{2+}$ dimer located at different B-acid pair sites calculated at the BLYP/DNP level based on 6T (10T) cluster models; the optimized structures and the potential energies of the transition state and product for methane C−H bond dissociation. This material is available free of charge via the Internet at http://pubs.acs.org.

References and Notes

(1) Wang, L.; Tao, L.; Xie, M.; Xu, G. *Catal. Lett.* **1993**, *21*, 35.
(2) Solymosi, F.; Erdohelyi, A.; Szoke, A. *Catal. Lett.* **1995**, *32*, 43.
(3) Wang, D.; Lunsford, J. H.; Rosynek, M. P. *Top. Catal.* **1996**, *3*, 289.
(4) Liu, S.; Dong, Q.; Ohnishi, R.; Ichikawa, M. *J. Chem. Soc., Chem. Commum.* **1997**, 1455.
(5) Shu, J.; Adnot, A.; Grandjean, B. P. A. *Ind. Eng. Chem. Res.* **1999**, *38*, 3860.
(6) Wong, S.; Xu, Y.; Liu, W.; Wang, L.; Guo, X. *Appl. Catal., A* **1996**, *136*, 7
(7) Wang, L.; Xu, Y.; Xie, M.; Liu, S.; Tao, L. *Stud. Surf. Sci. Catal.* **1995**, *94*, 495.
(8) Szoke, A.; Solymosi, F. *Appl. Catal., A* **1996**, *142*, 361.
(9) Solymosi, F.; Cserenyi, J.; Szoke, A.; Bánsági, T.; Oszkó, A. *J. Catal.* **1997**, *165*, 150.
(10) Wang, D.; Lunsford, J. H.; Rosynek, M. P. *Top. Catal.* **1996**, *3*, 289.
(11) Wang, D.; Lunsford, J. H.; Rosynek, M. P. *J. Catal.* **1997**, *169*, 347.
(12) Li, W.; Meitzner, G. D.; Borry, R. W., III; Iglesia, E. *J. Catal.* **2000**, *191*, 373.
(13) Stakheev, A. Y.; Khodakov, A. V.; Kustov, L. M.; Kazansky, V. B.; Minachev, Kh. M. *Zeolite* **1992**, *12*, 866.
(14) Xu, Y.; Shu, Y.; Liu, S.; Huang, J.; Guo, X. *Catal. Lett.* **1995**, *35*, 233.

(15) Vahel, A.; Hubener, S.; Eichler, B. *Radiochim. Acta* **1995**, *69*, 233.
(16) Vahel, A.; Hubener, S.; Dressler, R.; Eichler, B.; Turler, A. *Radiochim. Acta* **1997**, *78*, 53.
(17) Zhou, D.; Ma, D.; Liu, X.; Bao, X. *J. Mol. Catal. A: Chem* **2001**, *168*, 225.
(18) Ma, D.; Shu, Y.; Bao, X.; Xu, Y. *J. Catal.* **2000**, *189*, 314.
(19) Wang, D.; Rosynek, M. P.; Lunsford, J. H. *J. Catal.* **1997**, *169*, 347.
(20) Chen, L.; Lin, L.; Xu, Z.; Lian, X.; Zhang, T.; Li, X. *J. Catal.* **1995**, *157*, 190.
(21) Xu, Y.; Liu, S.; Wang, L.; Xie, M.; Guo, X. *Catal. Lett.* **1995**, *30*, 135.
(22) Xu, Y.; Liu, W.; Wong, S. T.; Wang, L.; Guo, X. *Catal. Lett.* **1996**, *40*, 207.
(23) Solymosi, F.; Szoke, A.; Cserenyi, J. *Catal. Lett.* **1996**, *39*, 157.
(24) Schurman, Y.; Decamp, T.; Pantazidis, A.; Xu, Y. D.; Mirodatos, C. *Stud. Surf. Sci. Catal.* **1997**, *109*, 351.
(25) Ma, D.; Han, X. W.; Zhou, D. H.; Yan, Z. M.; Fu, R. Q.; Xu, Y. D.; Bao, X. H.; Hu, H. B.; Au-Yueng, S. C. F. *Chem.—Eur. J.* **2002**, *8*, 4557.
(26) Ma, D; Zhu, Q. J; Wu, Z. L; Zhou, D. H; Shu, Y. Y; Xin, Q; Xu, Y. D; Bao, X. H. *Phys. Chem. Chem. Phys.* **2005**, *7*, 3102.
(27) Borry, R. W., III; Kim, Y. H.; Huffsmith, A.; Reimer, J. A.; Iglesia, E. *J. Phys. Chem. B* **1999**, *103*, 5787.
(28) Ding, W.; Li, S.; Meitzner, G. D.; Iglesia, E. *J. Phys. Chem. B* **2001**, *105*, 506.
(29) Kim, Y. H.; Borry, R. W., III; Iglesia, E. *J. Ind. Eng. Chem.* **2000**, *6*, 72.
(30) Kim, Y. H.; Borry R. W., III; Iglesia, E. *Microporous Mesoporous Mater.* **2000**, *35*−*36*, 495.
(31) Rice, M. J.; Chakraborty, A. K.; Bell, A. T. *J. Catal.* **1999**, *186*, 222.
(32) Tessonnier, J. P.; Louis, B.; Walspurger, S.; Sommer, J.; Ledoux, M. J.; Pham-Huu, C. *J. Phys. Chem. B* **2006**, *110*, 10390.
(33) Minming, H.; Howe, R. F. *J. Catal.* **1987**, *108*, 283.
(34) Zhang, J.-Z.; Long, M. A.; Howe, R. F. *Catal. Today* **1998**, *44*, 293.
(35) Liu, H.; Shen, W.; Bao, X.; Xu, Y. *Appl. Catal., A* **2005**, *295*, 79.
(36) Frisch, M. J.; Trucks, G. W.; Schlegel, H. B.; Scuseria, G. E.; Robb, M. A.; Cheeseman, J. R.; Montgomery, J. A., Jr.; Vreven, T.; Kudin, K. N.; Burant, J. C.; Millam, J. M.; Iyengar, S. S.; Tomasi, J.; Barone, V.; Mennucci, B.; Cossi, M.; Scalmani, G.; Rega, N.; Petersson, G. A.; Nakatsuji, H.; Hada, M.; Ehara, M.; Toyota, K.; Fukuda, R.; Hasegawa, J.; Ishida, M.; Nakajima, T.; Honda, Y.; Kitao, O.; Nakai, H.; Klene, M.; Li, X.; Knox, J. E.; Hratchian, H. P.; Cross, J. B.; Bakken, V.; Adamo, C.; Jaramillo, J.; Gomperts, R.; Stratmann, R. E.; Yazyev, O.; Austin, A. J.; Cammi, R.; Pomelli, C.; Ochterski, J. W.; Ayala, P. Y.; Morokuma, K.; Voth, G. A.; Salvador, P.; Dannenberg, J. J.; Zakrzewski, V. G.; Dapprich, S.; Daniels, A. D.; Strain, M. C.; Farkas, O.; Malick, D. K.; Rabuck, A. D.; Raghavachari, K.; Foresman, J. B.; Ortiz, J. V.; Cui, Q.; Baboul, A. G.; Clifford, S.; Cioslowski, J.; Stefanov, B. B.; Liu, G.; Liashenko, A.; Piskorz, P.; Komaromi, I.; Martin, R. L.; Fox, D. J.; Keith, T.; Al-Laham, M. A.; Peng, C. Y.; Nanayakkara, A.; Challacombe, M.; Gill, P. M. W.; Johnson, B.; Chen, W.; Wong, M. W.; Gonzalez, C.; Pople, J. A. *Gaussian 03*, revision C.02; Gaussian, Inc.: Wallingford, CT, 2004.
(37) Material Studio, Version 2.2.1, Accelrys Inc., 2002.
(38) Perdew, J. P.; Wang, Y. *Phys. Rev. B* **1992**, *45*, 13244.
(39) Becke, A. *J. Chem. Phys.* **1988,** *88, 2547*.
(40) Lee, C.; Yang, W.; Parr, R. G. *Phys. Rev. B* **1988,** *37, 786.*
(41) Gordon, M. S. *Chem. Phys. Lett.* **1980**, *76*, 163.
(42) Hehre, W. J.; Ditchfield, R.; Pople, J. A. *J. Chem. Phys.* **1972**, *56*, 2257.
(43) Dolg, M.; Wedig, U.; Stoll, H.; Preuss, H. *J. Chem. Phys.* **1987**, *86*, 866.
(44) Bergner, A.; Dolg, M.; Kuechle, W.; Stoll, H.; Preuss, H. *Mol. Phys.* **1993**, *80*, 1431.
(45) Scott, A. C.; Radom, L. *J. Chem. Phys.* **1996**, *100*, 16502.
(46) Foster, J. P.; Weinhold, F. *J. Am. Chem. Soc.* **1980**, *102*, 7211.
(47) Reed, A. E.; Weinstock, R. B.; Weinhold, F. *J. Chem. Phys.* **1985**, *83*, 735.
(48) Reed, A. E.; Curtiss, L. A.; Weinhold, F. *Chem. Rev.* **1988**, *88*, 899.
(49) Van Koningsveld, H.; Jansen, J. D.; an Bekkum, H. J. *Zeolites* **1990**, *10*, 236.
(50) Chatterjee, A.; Bhattacharya, D.; Chatterjee, M.; Iwasaki, T. *Microporous Mesoporous Mater.* **1999**, *32, 189.*
(51) Nicholas, J. B. *Top. Catal.* **1997**, *4*, 157.
(52) Koch, W.; Hertwig, R. H. *Chem. Phys. Lett.* **1997**, *286*, 345.
(53) Li, B.; Li, Sh. J.; Li, N.; Chen, H. Y.; Zhang, W. J.; Bao, X. H.; Lin, B. Ch. *Microporous Mesoporous Mater.* **2006**, *88*, 244.
(54) Broclawik, E.; Himei, H.; Yamadaya, M.; Kubo, M.; Miyamoto, A. *J. Chem. Phys.* **1995**, *103*, 2102.
(55) Nachrigall, P.; Nachtigallová, D.; Sauer, J. *J. Phys. Chem. B* **2000**, *104*, 1738.
(56) Barbosa, L. A. M. M.; Zhidomirov, G. M.; Van Santen, R. A. *Phys. Chem. Chem. Phys.* **2000**, *2*, 3909.
(57) Yakovlev, A. L.; Shubin, A. A.; Zhidomirov, G. M.; Van Santen, R. A. *Catal. Lett.* **2000**, *70*, 175.
(58) Spuhler, P.; Holthausen, M. C.; Nachtigallová, D.; Nachtigall, P.; Sauer, J. *Chem.—Eur. J.* **2002**, *8*, 2009.
(59) Lacheen, H. S.; Iglesia, E. *J. Phys. Chem. B* **2006**, *110*, 5462.
(60) Zhou, D. H.; Ma, D.; Wang, Y.; Liu, X. C.; Bao, X. H. *Chem. Phys. Lett.* **2003**, *373*, 46.
(61) Pine, L. A.; Maher, P. J.; Wachter, W. A. *J. Catal.* **1984**, *85*, 466.
(62) Teraishi, K.; Akanuma, K. *J. Phys. Chem. B* **1997**, *101*, 1298.
(63) Schröder, K.-P.; Sauer, J. *J. Phys. Chem.* **1993**, *97*, 6579.
(64) Kramer, G. J.; Van Santen, R. A. *J. Am. Chem. Soc.* **1993**, *115*, 2887.
(65) Wang, Y.; Zhou, D. H.; Yang, G.; Miao, Sh. J.; Liu, X. Ch.; Ma, D.; Bao, X. H. *J. Phys. Chem. A* **2004**, *108*, 6730.
(66) Zhou, D. H.; He, N.; Wang, Y. Q.; Yang, G.; Liu, X. C.; Bao, X. H. *J. Mol. Struct.*: *THEOCHEM* **2006**, *756*, 39.
(67) Zhou, D. H.; Ma, D.; Liu, X. C.; Bao, X. H. *J. Chem. Phys.* **2001**, *114*, 9125.
(68) Fu, G.; Xu, X,; Lu, X.; Wan, H. L. *J. Am. Chem. Soc.* **2005**, *127*, 3989.